Plasmon Dynamics in Colloidal Cu 2– x Se Nanocrystals

Ajay Ram, Srimath Kandada, Francesco Scotognella, Giuseppe Della Valle, Ajay Ram Srimath Kandada, Dirk Dorfs, Margherita Zavelani-Rossi, Matteo Conforti, Guglielmo Lanzani, Liberato Manna, et al.

Plasmon dynamics in colloidal $Cu_{2-x}Se$ nanocrystals

Francesco Scotognella§, Giuseppe Della Valle§, Ajay Ram Srimath Kandada§, Dirk Dorfs, Margherita Zavelani-Rossi, Matteo Conforti, Guglielmo Lanzani, Liberato Manna, Francesco Tassone*

§ F. S., G. D. V. and A. R. S. K. equally contributed to this work.

* To whom correspondence should be addressed: francesco.scotognella@polimi.it

Theoretical and experimental research on the optical features exhibited by metallic nano-systems has paved the way to extensive applications in several fields, from surface-enhanced spectroscopies, to biological and chemical nano-sensing. Such developments are primarily due to the localized plasmon resonances (LPR), resulting in intense optical absorption and scattering as well as sub-wavelength localization of large electrical fields in the vicinity of the nano-object. [1-9] The plasmonic response of these metallic nanostructures is strongly dependent on the type of metal of which they are made, on the dielectric function of the surrounding medium, on the particle shape and, to a lesser extent, it is also dependent on the particle size. However, for ultra-small nanoparticles, size dependent effects are negligible, and for homogeneous (i.e. purely metallic) structures, the plasmonic resonance is only determined by the properties of the metal. Since few metallic materials such as Ag, Au, Cu and Pt have been successfully shaped into ultra-small nanoparticles, [10-14] plasmonic response has been mostly reported in the visible, with the exception of some Au-based elongated nanostructures which have also demonstrated plasmonic response in the near infra-red (~800 nm). [15-16]

In order to circumvent such a limitation, a consistent effort has been spent in the last years in the synthesis of heavily-doped semiconductor nanocrystals so as to achieve metallic behaviour and eventually a tunable plasmonic response in a broader optical spectrum. In particular, research was concentrated onto S-based, Se-based and Te-based II-VI semiconductor nanocrystals with Cd-Cu substitution. [17-22] In these nanoparticles Copper can exist in a wide range of stoichiometric ratios in addition to the 2:1 with respect to Selenium or Sulfur, resulting into Copper vacancies and into "self-doping" of the material. The influence of this heavy doping on the optical response in the infrared region has been a subject of interest in the last decade. In 1973, Gorbachev and Putilin observed a plasmon band in the reflectivity of p-type copper selenide and copper telluride thin films. [23] They also found that the spectral position of this band strongly depends on temperature, a fact that they attributed to a strong dependence of the hole effective mass on temperature. Very recently, Alivisatos and coworkers [22] and Manna and coworkers [24] reported a detailed study on plasmonic properties of

Cu_2X nanocrystals (with S in [22] and Se in [24], respectively), which showed how starting from nearly stoichiometric Cu_2X particles, their oxidation (upon exposure on air) increased the degree of Copper deficiency leading to the emergence of an IR band that gradually increased in intensity and blue-shifted in energy. Manna et al. also showed the *reversible tuning* of the IR plasmonic response of $Cu_{2-x}Se$ nanocrystals via their gradual oxidation, either under air or by stepwise addition of a Ce(IV) complex. [24]

In the very last years, the dynamical response of plasmonic nano-structures has also attracted more and more attention, giving rise to the emerging field of *ultra-fast active plasmonics* [25]. Actually, it has been recently reported that direct optical excitation of the metal by intense femtosecond laser pulses lead to ultra-fast modulation of plasmonic signals, thus resulting in unprecedented terahertz modulation bandwidth, a speed at least five orders of magnitude faster than existing technologies. [25] A quantitative investigation of such dynamical features is thus of the most importance for the development of next generation of ultra-fast nano-devices. Pump-probe spectroscopy, giving access to the electronic excitation and subsequent relaxation processes in the material, has been demonstrated to be the eligible tool for the experimental study of the ultra-fast dynamical features exhibited by plasmonic nanostructures. So far, several noble metal sctructures have been investigated, including spherical particles [26-28], as well as nanorods [29], leading to a general scenario of the underlying physical phenomena similar to the one observed in bulk (i.e. thin film) metallic systems [30,31]. Actually, when the pump pulse is in the infrared the initial Fermi distribution of electrons in the conduction band is strongly perturbed by pump absorption; the pump pulse creates *energetic electrons* that are not in thermal equilibrium and within few hundred fs a new Fermi distribution is achieved by strong electron-electron scattering, resulting in a thermalized electron gas with higher temperature than the lattice (*hot electrons*); subsequently, within the next few ps the electron gas cools down by releasing its excess energy to the lattice through electron-phonon coupling; and, ultimately, within hundred of ps, the nanoparticle releases its energy to the environment, [16] (with heat conduction to the surface of the nanoparticles provided by phonon-phonon coupling).

In this work, we report on the optical response of $Cu_{2-x}Se$ colloidal nanocrystals to ultrafast laser pulses, recorded via pump-probe experiments in the infra-red with 200 fs resolution time. In particular we investigated the hole-phonon coupling dynamics taking place in the ps time scale. The experimental results are interpreted according to the two-temperature model already developed for the theoretical investigation of more conventional metallic systems.

The $Cu_{2-x}Se$ nanocrystals considered in the present study have been prepared following the synthesis process reported in [24]. As already demonstrated, the optical response exhibited by these nanostructures under continuous wave excitation with infra-red light is plasmonic in nature and can be quantitatively interpreted according to quasi-static approximation of the Mie theory [24]. More precisely, the dipolar absorption and scattering cross-sections of a $Cu_{2-x}Se$ nanoparticle of radius $R << 2\pi c/\omega$ are respectively given by:

$$\sigma_A = 4\pi k R^3 \cdot \mathrm{Im}\left\{\frac{\varepsilon(\omega)-\varepsilon_m}{\varepsilon(\omega)+2\varepsilon_m}\right\}$$
$$\sigma_S = \frac{8}{3}\pi k^4 R^6 \left|\frac{\varepsilon(\omega)-\varepsilon_m}{\varepsilon(\omega)+2\varepsilon_m}\right|^2 \qquad (1)$$

where $\varepsilon_m = n_m^2$ is the dielectric constant of the environmental medium, $k = n_m\,\omega/c$ and $\varepsilon = \varepsilon_1(\omega) + i\varepsilon_2(\omega)$ is the $Cu_{2-x}Se$ dielectric function provided by the Drude model:

$$\varepsilon_1 = \varepsilon_\infty - \frac{\omega_p^2}{\omega^2+\Gamma^2}$$
$$\varepsilon_2 = \frac{\omega_p^2\Gamma}{\omega\left(\omega^2+\Gamma^2\right)} \qquad (2)$$

with ε_∞ the high frequency dielectric permittivity (due to the presence of inter-band transitions at a higher photon energy), ω_p the plasma frequency of the free carriers of the system, and Γ the free carrier damping (i.e. the inverse of the carrier relaxation time).

Our previous results [24] showed that, depending on the 'oxidation' parameter *x,* different material dielectric functions $\varepsilon$are retrieved, resulting in a plasmon resonance (at frequency ω_0 approximately

given by $\varepsilon_1(\omega_0) = -2\varepsilon_m$) that blue-shifts with increasing x. For the present study we selected $x = 0.15$ (i.e. $Cu_{1.85}Se$) samples leading to a large blue shift of the plasmon peak. We measured a relatively narrow plasmonic resonance, with an intense peak around 1050 nm, is measured for $Cu_{1.85}Se$ particles dispersed in toluene solution (refractive index $n_m = 1.505$, $\varepsilon_m = 2.25$), as illustrated in Figure 1, where we plot the optical density measured in a 1 mm thick quartz cuvette with an estimated particle concentration $N = 3\text{x}10^{13}$ cm^{-3}. Figure 1 also reports the total extinction cross-section $\sigma_E = \sigma_A + \sigma_S$ of $Cu_{1.85}Se$ nanoparticles computed from Eqs. (1)-(2) with Drude parameters $\varepsilon_\infty = 1.38$, $\omega_P = 4.43\text{x}10^{15}$ rad/s, and $\Gamma = 9.72\text{x}10^{14}$ rad/s, in agreement with our previous study [24].

The pump probe set-up is based on a commercial Ti:Sapphire amplified laser system delivering 150 fs pulses at 1 KHz repetition rate at a central wavelength of 800 nm. A fraction of the beam is used to pump a non-collinear parametric amplifier (NOPA) to generate pulses in the infra-red [32,33]; we tuned the NOPA to obtain pump pulses in correspondence with the plasmonic resonance of the sample (~1050 nm, 1.19 eV with a bandwidth of 40 nm). The probe pulses are produced by focusing the fundamental beam into a 2 mm thick sapphire plate to generate a stable white light super-continuum. A long pass filter with cut-on wavelength at 820 nm is used to filter out the residual fundamental and the visible component of the probe pulses. The pump and probe beams are focused onto the sample with a spot size of 200 μm. The pump-probe setup, employs a computer controlled optical multichannel analyser and the measured signal is a map of the chirp-free differential transmission $\Delta T/T = (T_{on} - T_{off}) / T_{off}$ as a function of wavelength and the pump-probe time delay; T_{on} and T_{off} are the probe spectra transmitted by the excited and unperturbed sample, respectively.

Figure 2 reports the temporal dynamics of the relative differential transmission ($\Delta T/T$) probed at 900 nm, obtained by exciting the nanocrystals with different pump fluencies. The experimental results reveal $\Delta T/T > 0$ right after the absorption of the pump beam, with maximum value of about 40% under the

maximum pump fluence of 2.23 mJ/cm^2. A monothonic and fast decrease of the signal is then observed within a few ps (Figure 2a) followed by a much slower (ns time scale) decay (Figure 2b), leading to complete recovery of the initial condition (before pump arrival) within few ns.

To tentatively describe the non-linear optical features as reported in Fig. 2 we applied the theoretical methods developed for metals, since the linear optical response of $Cu_{2-x}Se$ nanocrystals is dominated by the metallic behaviour of the system, which leads to a plasmonic resonance in the extinction spectrum, we applied the theoretical methods developed for metals to tentatively describe the non-linear optical features as reported in Figure 2.

The pump-probe dynamics of metallic systems can be ascribed to the variations attained by the metal dielectric function induced by pump absorption. [30,31] As explained before, the ps dynamics is related to the cooling of the hot electron gas generated by absorption of the pump energy. Therefore, the time evolution of the system wihin ps time scale can be modelled as a heat transfer between a thermalized gas of carriers at temperature T_C and the lattice at a lower temperature T_L, via carrier-phonon scattering process. The so-called Two Temperature Model (TTM) quantitatively accounts for such transfer according to the following coupled equations [30]:

$$\begin{cases} \gamma T_C \dfrac{dT_C}{dt} = -G(T_C - T_0) + P_A(t) \\ C_L \dfrac{dT_L}{dt} = G(T_C - T_L) - G_L(T_L - T_0) \end{cases} \qquad (3)$$

where γT_C is the heat capacity of the carrier gas, being γ the so-called carrier heat capacity constant, C_L is the heat capacity of the lattice, G is the carrier-lattice coupling factor, G_L is the lattice-environment coupling factor, T_0 is the environmental temperature (which is supposed to be constant) and $P_A(t)$ is the pump power density absorbed in the volume of the metallic system. Once the temperature dynamics induced by the pump pulse is determined from Eq. (3), the optical response of the systems to the probe pulse can then be retrieved from the temperature dependence of the dielectric function of the material

and from the electromagnetic boundary conditions due to the particular geometry of the system, which in the case of a small spherical particle are described by Eq. (1).

The effects of the carrier and lattice temperatures on the dielectric function also depend on the detailed band structure of the material, and on the energy of the probe photon. Little is known on the band structure of $Cu_{2-x}Se$, apart from the fact that it behaves as a p-type degenerate semiconductor with half filled valence band. [34,24] Moreover, many possible crystallographic phases of $Cu_{2-x}Se$ have also been found. [35] Here we report in Figure 3.a a tentative and qualitative sketch of the band structure deduced from spectroscopical investigations reported in the literature. According to Al-Mamun et. al. [36], the $Cu_{2-x}Se$ system with $x = 0.15$ exhibits two interband optical transitions, a direct transition at 2.1 eV and an indirect transition at 1.3 eV. It is thus expected that the pump photon at 1.19 eV energy is absorbed by an intra-band process similarly to what happens in noble metals in the infra-red. The subsequent heating of the carrier gas results in a smearing of the Fermi distribution, and gives rise to a modulation of the inter-band transition probability for the probe light at 1.38 eV (Figure 3.a), which results in a modulation $\Delta\varepsilon_\infty$ of the ε_∞ parameter in the Drude dielectric function Eq. (2). Being the probe photon energy here used much lower than the direct inter-band transition edge, and considering that the indirect inter-band process, and its modulation, is much weaker compared to direct transitions, we conclude that the imaginary part of $\Delta\varepsilon_\infty$ is negligible compared to the real part. In metals, it is well known that this modulation is proportional to the carrier excess energy [28,31], and thus it scales quadratically with the carrier temperature T_C, i.e. $\Delta\varepsilon_\infty = \delta T_C^2$, δ being a fitting parameter.

Not only the carrier temperature but also the lattice temperature results in a modulation of the dielectric function ε_∞. In metallic systems the Drude damping Γ factor increases linearly with T_L. However, the resulting temperature dependence of the dielectric function ε is relatively weak and tipically negligible, unless the lattice temperature is increased significantly. Instead $Cu_{2-x}Se$ exhibits the additional and

distinctive dependence of the hole mass on the lattice temperature as reported by Gorbachev and Putilin. [23] This dependence on the temperature is much stronger compared to the modulation of Γ. For the aims of the present work, we retrieved an analytical expression for such dependence by simply fitting the data reported in [23], providing the following formula for the hole effective mass: $m_h(T_L) = (aT_L^b + c)\, m_0$, with $a = 4.04\text{x}10^{-16}$ (K^{-b}), $b = 5.71$, $c = 0.151$, and m_0 the free electron mass. The temperature dependence of m_h results in a temperature dependence of the plasma frequency of the form:

$$\omega_P(T_L) = [N_C e^2 / m_h(T_L)\varepsilon_0]^{1/2} \qquad (4)$$

Therefore the plasma frequency decreases as the lattice is heated (N_C being the free carrier density). The effect on the extinction cross-section, numerically computed from quasi-static formulas given in Eq. (1) is illustrated in Figure 3b. Note that for the probe wavelength of 900 nm the extinction is strongly reduced as the lattice is heated by just few tens of degrees.

The previous discussion provides a qualitative understanding of the dynamics observed in the experimental data reported in Figure 2.a: the T_C dependent inter-band effect, resulting in an increase of the real part of the dielectric function ε of the material, leads to a red-shift of the plasmonic resonance (which is now provided by $\varepsilon_1(\omega_0) + \Delta\varepsilon_\infty = -2\varepsilon_m$), and thus enhances the transmissivity of the probe (which is in the blue-tail of the extinction spectrum, Figure 1) right after the pump absorpion; the T_L dependent intra-band effect, due to the temperature dependence of the free carrier effective mass, also results in a red shift of the plasmonic resonance, and is related to the long-living differential transmission tail which can be observed after the end of the carrier-lattice interaction, and for several ps. The long time-scale dynamics (Figure 2.b) is thus completely decoupled from the fast carrier-phonon dynamics, and thus an exponential decay with a time constant $1/G_L$ is expected.

In order to attempt a quantitative comparison with the experiment, the theoretical differential transmission was computed as $\Delta T/T = \exp(-\Delta\sigma_E NL) - 1$, $\Delta\sigma_E$ being the variation attained by the

extinction cross-section according to the quasi-static formulas of Eq.(1), and the temperature-dependent dielectric function of $Cu_{2-x}Se$ given by:

$$\varepsilon(T_C,T_L)=\varepsilon_\infty+\Delta\varepsilon_\infty(T_C)-\frac{\omega_P(T_L)}{\omega^2+\Gamma^{-2}}+i\frac{\Gamma\omega_P(T_L)}{\omega\left(\omega^2+\Gamma^{-2}\right)} \quad (5)$$

with T_C and T_L provided by numerical solution of the TTM, and G, δ, and G_L for the long time-scale dynamics, as fitting parameters. In doing so, we assumed a heat capacity of the lattice $C_L = 2.72\text{x}10^6$ J m^{-3} K^{-1}, according to the experimental data reported in [35] for α-Cu_2Se, whereas the heat capacity of the carriers was estimated as $\gamma = r\gamma_{Au} = 1.37$ J m^{-3} K^{-2}, with $\gamma_{Au} = 62.9$ J m^{-3} K^{-2} being the heat capacity of the free electrons in Gold and r the ratio between Cu_2Se carrier density (estimated, from the plasma frequency and hole effective mass at room temperature, to be $N_C = \omega_P^2\varepsilon_0 m_h(T_C)/e^2 = 1.28\text{x}10^{27}$ cm^{-3}) and gold carrier density ($5.9\text{x}10^{28}$ cm^{-3}).

Given the incident pump fluences of 96, 318 and 2230 μJ/cm^2, the absorbed pump power density $P_A(t)$ was estimated from pump absorption measurements, showing that only 1% of the incident pump energy is absorbed by the sample, despite the pump wavelength is at the peak of the linear absorption of $Cu_{1.85}Se$ nanoparticles. This indicates that the high fluence of the pump leads to strongly non-linear absorption phenomena even during the pump pulse. Such phenomena might be related to the strong perturbation of the plasmonic regime due to energetic and non-thermalized carriers, which could lead to a substantial shift of the plasmonic resonance, and/or to a substantial smearing, so as to drastically reduce the absorption cross-section at the pump wavelength. The absorption dynamics is thus expected to be dominated by the non-thermalized carrier dynamics, which occurs in the tens of fs time scale and is far beyond the resolution time of the present experiment.

Numerical solution of the TTM model with the best fitting parameters is reported in Figure 4a, whereas the corresponding numerically computed differential transmission is shown in Figure 2.a (for the ps

time scale) and in Figure 2.b (for the long-time scale). We estimated a low temperature carrier-phonon coupling factor $G = G_0 = 2.0\text{x}10^{15}$ W m^{-3}K^{-1}, which is one order of magniture lower than in Gold. Since the G_0 factor is proportional to the carrier density [37], this lower G is in agreement with the much lower carrier density in $Cu_{1.85}Se$ compared to gold. We also estimated $\delta = 5\text{x}10^{-8}$ K^{-2}, which is about 40% higher than in silver structures at 900 nm probe wavelength [31].

Note that numerical simulations are in good agreement with the experimental data for the lower pump fluences whereas the higher fluence results in some quantitative misagreement within the short time-scale dynamics (compare solid and dotted green curves in Figure 2a). Actually for such a high fluence the TTM predicts a carrier temperature increase exceeding 3000 K (see green curves in Figure 4a). It is thus expected that, similarly to what happens in noble metals, the carrier heat capacity γ and the electron-phonon coupling factor G are no more temperature independent [37]. We found that by tentatively introducing temperature dependences for γ and G that mimick the temperature dependences reported for Gold at high temperatures [37], i.e. $\gamma=\gamma_0+\beta_1(T_C-T_G)$ and $G = G_0+\beta_2(T_C-T_G)^3$ for $T_C > T_G$, with β_1, β_2 and T_G fitting parameters, a much better agreement between the model and the experiment is found also for the higher pump fluence (see dashed green curve in Figure 2.a, and see Figure 4.c for fitted temperature dependent parameters). However, being γ and G strongly dependent on the actual DOS of the free carriers [37], a quantitative determination of their temperature dependence can not be asserted without a better knowledge of the band structure of the $Cu_{1.85}Se$ crystal, which is out of the scope of the present work.

In conclusion, we report the first observation of the ultrafast optical response of $Cu_{2-x}Se$ nanoparticles excited at the plasmon resonant energy. We have been able to quantitatively describe the optical response, and to extract from it the electron-phonon coupling constant, which compares reasonably well with those found in noble metals after accounting for the lower carrier density. We remark that the

relatively low carrier density and structural peculiarities of $Cu_{2-x}Se$ lead to significant deviations of the response from the well-known behaviour found in the more traditional metallic nanoparticles (for example the noble metal nanoparticles). In particular, the lower carrier density is responsible for a lower carrier heat capacity and for a much larger effective carrier temperatures at comparable fluences. This leads to strong non-linear effects at high fluences both during the pump absorption process, and during the carrier temperature relaxation process. Moreover, the large temperature dependence of the hole effective mass results into large residual differential transmission signals due to significant shifts of the plasmonic resonance. Such a marked temperature dependence of the hole mass is possibly related to the complex phase diagram of $Cu_{2-x}Se$ [35], to incipient changes of the crystalline phase, and to a strong sensitivity of the valence band shape on this change of phase. From a technological point of view, this material can be promising, as an example, for the development of ultrafast nano-devices operating at terahertz modulation bandwidth, [25] with the peculiar advantage of plasmon resonance tunability in the IR region, with potential interest for telecom applications.

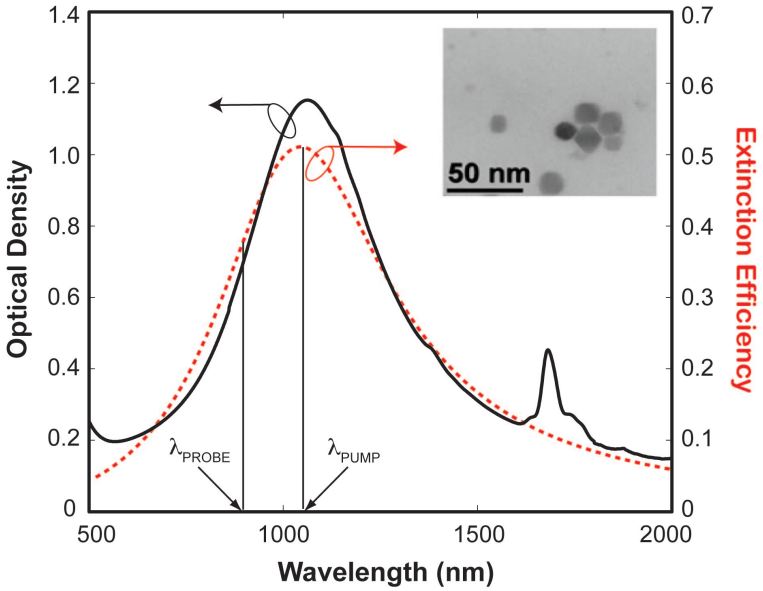

Figure 1. Experimental optical density spectrum of the $Cu_{1.85}Se$ nanoparticles dispersed in toluene solution from extinction measurements in continuous wave (black solid line), and theoretically computed extinction efficiency (red dashed line) from dielectric function data reported in [24]. The narrow peal at around 1700 nm is due to toluene absorption. Arrows indicate the wavelength of the optical pulses in the pump-probe experiments. Inset shows a TEM image of the nanoparticles.

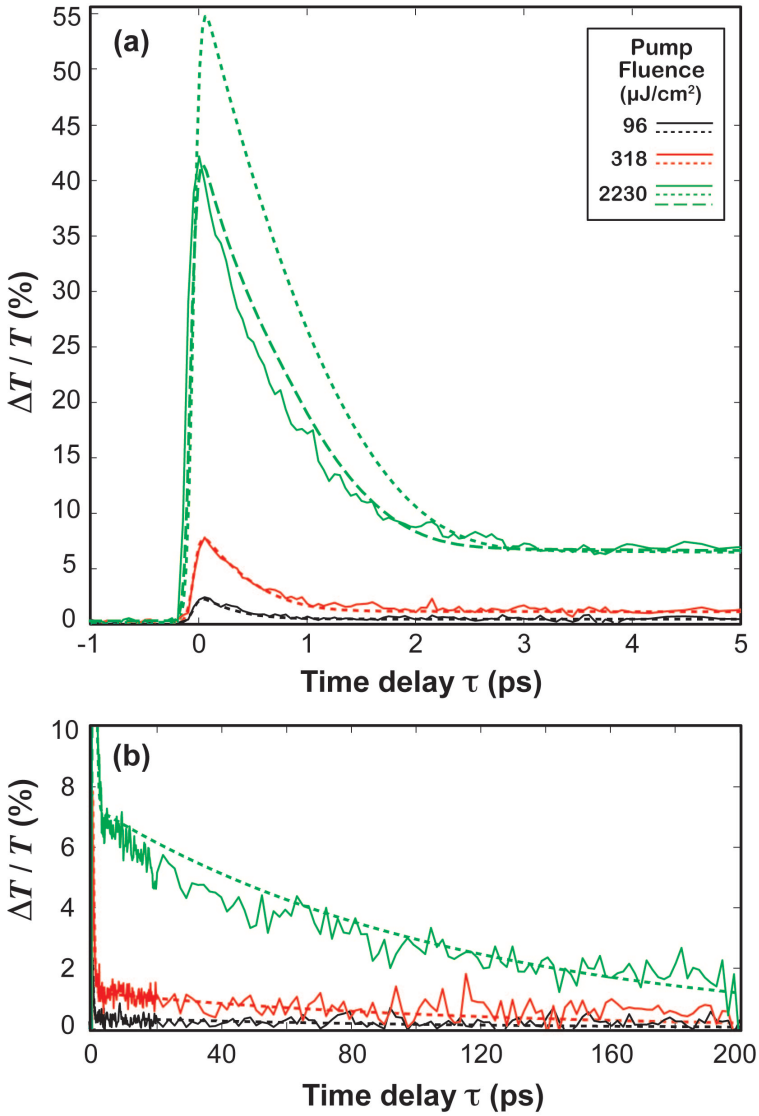

Figure 2. Differential transmission signal from $Cu_{2-x}Se$ nanocrystal dispersion in toluene for (a) short-time dynamics and (b) long-time dynamics. Experimental results (solid lines) are compared with numerical calculations (dotted and dashed lines) for three different incident pump fluences.

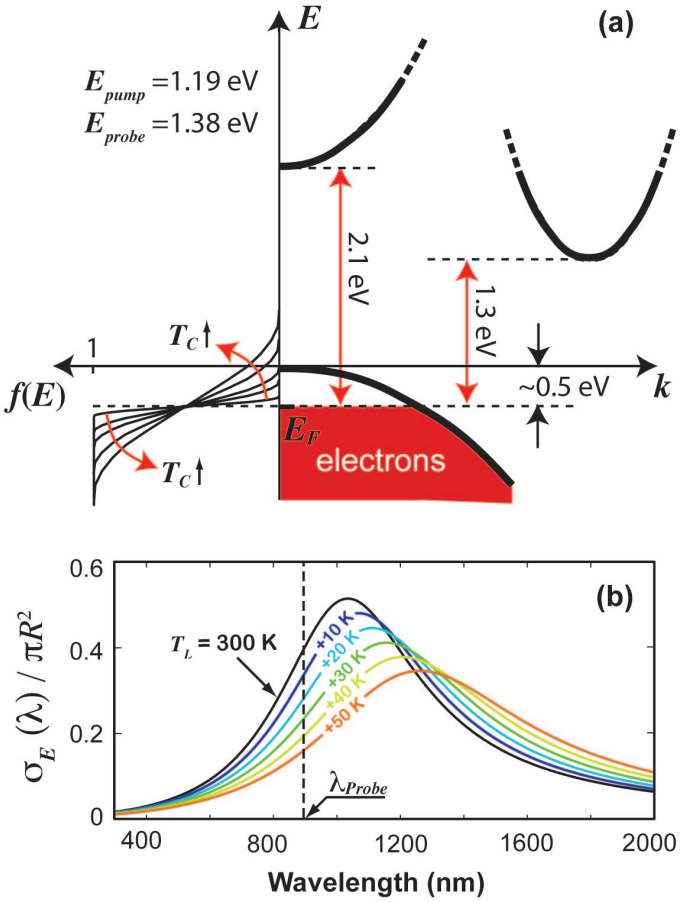

Figure 3. (a) Tentative sketch of $Cu_{2-x}Se$ band diagram for optical transitions in the visible. Smearing of the electron distribution $f(E)$ due to intra-band pump absorption and subsequent carrier temperature (T_C) increase is also illustrated. (b) Extinction cross-section of $Cu_{2-x}Se$ nano-spheres at different lattice temperatures (T_L) resulting from the carrier effective mass temperature dependence reported in [23].

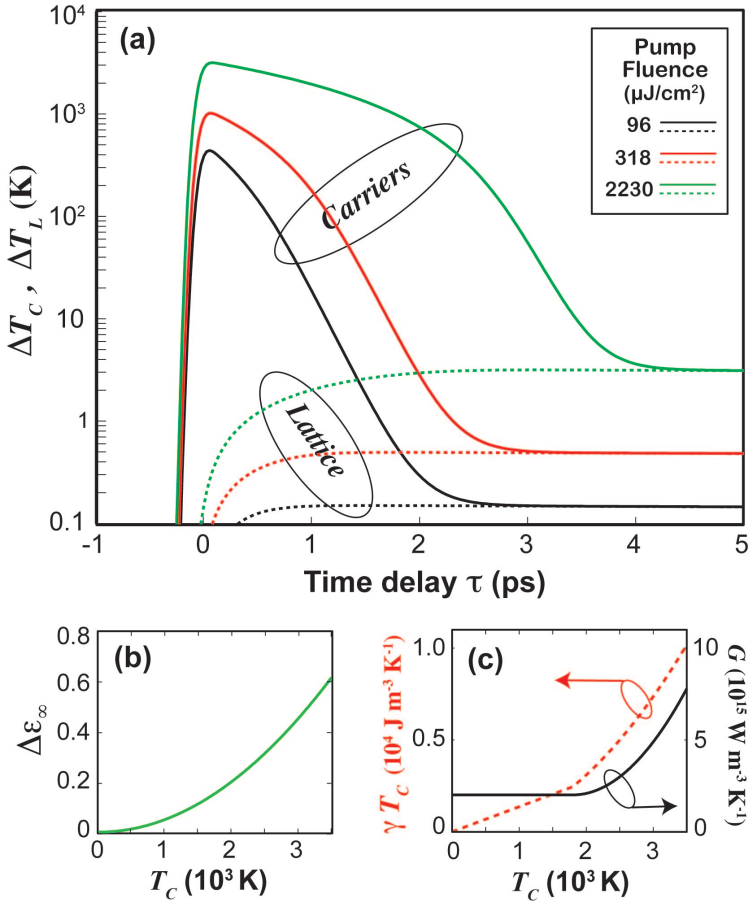

Figure 4. (a) Carrier (hole) and lattice temperature numerically computed from the TTM of Eq. (3). (b) Interband dielectric permittivity $\Delta\varepsilon_\infty = \delta T_C^2$. (c) Hole heat capacity $\gamma T_C = [\gamma_0+\beta_1(T_C-T_G)]T_C$, and hole-phonon coupling parameter $G = G_0+\beta_2(T_C-T_G)^3$. Fitted parameters: $\delta = 5\text{x}10^{-8}$ K^{-2}; $G_0 = 2.0\text{x}10^{15}$ W m^{-3} K^{-1}; $\beta_1 = 9.08\text{x}10^{-4}$ W m^{-3} K^{-3}, $\beta_2 = 2\text{x}10^{9}$ W m^{-3} K^{-4}; $G_L = 25\text{x}10^{15}$ W m^{-3} K^{-1}.

REFERENCES

[1] Schmid, G. *Clusters and colloids: from theory to applications*, VCH: Weinheim, **1994**.

[2] Tam, F.; Goodrich, G. P.; Johnson, B. R.; Halas, N. J. *Nano Lett*. **2007**, *7*, 496–501.

[3] Templeton, A. C.; Wuelfing, W. P.; Murray, R. W. *Acc. Chem. Res*. **2000**, 33, 27.

[4] *Metal nanoparticles: synthesis, characterization, and applications*; Feldheim, D. L., Foss, C. A., Jr., Eds.; Marcel Dekker: New York, **2002**.

[5] Zeman E. J.; Schatz, G. C. *J. Phys. Chem*. **1987**, 91, 634–643.

[6] Emory, S. R.; Nie, S. *Science* **1997**, 275, 1102–1106.

[7] Haes, A. J.; Chang, L.; Klein, W. L.; Van Duyne, R. P. *J. Am. Chem. Soc*.**2005**, 127, 2264–2271.

[8] Raschke, G.; Kowarik, S.; Franzl, T.; Soennichsen, C.; Klar, T. A.; Feldmann, J.; Nichtl, A., Kurzinger, K. *Nano Lett*. **2003**, 3, 935–938.

[9] Englebienne, P. *Analyst* **1998**, 123, 1599–1603.

[10] Bastys, V.; Pastoriza-Santos I.; Rodriguez-Gonzalez, B.; Vaisnoras, R.; Liz-Marzan, L. M. *Adv. Func. Mater*. **2006**, 16, 6, 766-773.

[11] Link, S.; Wang, Z. L.; El-Sayed, M. A. *J, Phys. Chem B***1999**, 103, 18, 3529-3533.

[12] Klar, T.; Perner, M.; Grosse, S.; von Plessen, G.; Spirkl, W.; Feldmann, J. *Phys. Rev. Lett*., **1998**, 80, 19, 4249-4252.

[13] Bigall, N. C.; Hartling, T.; Klose, M.; Simon, P.; Eng, L. M.; Eychmuller, A. *Nano Lett*. **2008**, 8, 12, 4588-4592.

[14] Chan, G. H.; Zhao, J.; Hicks, E. M.; Schatz, G. C.; Van Duyne, R. P. *Nano Lett*. **2007**, 7, 7, 1947-1952.

[15] Bardham, R.; Grady, N. K.; Halas, N. J. *ACS Nano* **2009**, 3, 3, 744-752.

[16] Krahne, R.; Morello, G.; Figuerola, A.; George, C; Manna, L. *Phys*. *Rep*. **2011**, 501, 75-221.

[17] Deka, S.; Genovese, A.; Yang, Z.; Miszta, K.; Bertoni, G.; Krahne, R.; Giannini, C.; Manna, L. *J*. *Amer*. *Chem*. *Soc*. **2010**, 132, 26, 8912-8914.

[18] Choi, J.; Kang, N.; Yang, H. Y.; Kim, H. J.; Son, S. U. *Chem*. *Mat*. **2010**, 22, 12, 3586-3588.

[19] Zhao, Y. X.; Pan, H. C.; Lou, Y. B.; Qiu, X. F.; Zhu, J. J.; Burda, C. *J*. *Amer*. *Chem*. *Soc*. **2009**, 131, 12, 4253-4261.

[20] Sadtler, B.; Demchenko, D. O.; Zheng, H.; Hughes, S. M.; Merkle, M. G.; Dahmen, U.; Wang, L. W.; Alivisatos, A. P. *J*. *Amer*. *Chem*. *Soc*. **2009**, 131, 14, 5285-5293.

[21] Riha, S. C.; Johnson, D. C.; Prieto, A. L. *J*. *Amer*. *Chem*. *Soc*. **2010**, 133, 5, 1383–1390.

[22] Luther, J. M.; Jain, P. K.; Ewers, T.; Alivisatos, A. P. *Nat*. *Mater*. **2011**, 10, 5, 361-366.

[23] Gorbachev, V. V.; Putilin, I. M. *Phys*. *Stat*. *Sol*. *A* **1973**, 16, 553-559.

[24] Dorfs, D.; Härtling, T.; Miszta, K.; Bigall, N. C.; Kim, M. R.; Genovese, A.; Falqui, A.; Povia, M.; Manna, L. *J*. *Am*. *Chem*. *Soc*. **2011**, *accepted*.

[25] MacDonald K. F.; Sámson Z. L.; Stockman M. I.; Zheludev N. I. *Nat*. *Photonics* **2009**, 3, 55-58.

[26] Averitt R. D.; Westcott S. L.; Halas N. J. *Phys*. *Rev*. *B* **1998** 58, 15, R10203-R10206.

[27] Muskens O. L.; Del Fatti N.; Vallée F. *Nano Lett*. **2006**, 6, 3, 552-556.

[28] Del Fatti, N.; Vallée, F.; Flytzanis, C.; Hamanaka, Y.; Nakamura, A. *Chem*. *Phys*. **2000**, 251, 215-226.

[29] Link S.; Burda C.; Mohamed M. B.; Nikoobakht B.; and El-Sayed M. A. *Phys. Rev. B* **2000**, 61, 9, 6086-6090.

[30] Sun, C.-K.; Vallée, F.; Acioli, L. H.; Ippen, E. P.; Fujimoto, J. G. *Phys. Rev. B* **1994**, 50(20), 15337-15348.

[31] Owens D. T.; Fuentes-Hernandez C.; Hales J. M.; Perry J. W.; and Kippelen B. *J. Appl. Phys.* **2010**, 107 123114-1-8.

[32] Cerullo, G.; De Silvestri, S. *Rev. Sci. Instrum.* **2003**, 74, 1-18.

[33] Manzoni, C.; Polli, D.; Cerullo, G. *Rev. Sci. Instrum.* **2006**, 77, 023103-1-9.

[34] Abdullaev, G. B.; Aliyarova, Z. A.; Asadov, G. A. *Phys. Stat. Sol.* **1967**, 21, 461-464.

[35] Glazov, V. M.; Pashinkin, A. S.; and Fedorov, V. A. *Inorg. Mat.* **2000**, 36, 7, 641-652.

[36] Al-Mamun, A. B.; Islam, M. O.; Bhuiyan, A. H. *J. Mat. Sci.: Mat. El.* **2005**, 16, 263-268.

[37] Lin, Z.; Zhigilei, L. V.; Celli, V. *Phys. Rev. B* **2008**, 77, 075133-1-17.